Behavior-type analysis of the polarized Raman spectra of halogen-perturbed interstitial hydrogen atoms in alkali halides

J. F. Zhou,* E. Goovaerts, and D. Schoemaker
Physics Department, University of Antwerp (Universitaire Instelling Antwerpen), B-2610 Wilrijk (Antwerp), Belgium
(Received 19 December 1983)

The behavior-type analysis method of the polarized Raman scattering intensities on preferentially or randomly oriented defects described in the preceding paper was applied to study two types of perturbed interstitial hydrogen atom (H_i^0) centers in alkali halides doped with halogen impurities Y^-, heavier than the host halogen ion X^-. This method allows one to determine the symmetry of the defect, the nature of its vibrational modes, and the components of the Raman tensor. In a series of six crystals we have identified the A_1 and E modes of the H_i^0 center perturbed by a single substitutional Y^- ion, the $H_i^0(Y^-)$ center, which possesses $C_{3v}[111]$ symmetry. Compared to the T_2 mode frequency of the unperturbed H_i^0 center the E mode is unshifted or slightly higher, while the A_1 mode exhibits a much larger (up to 14%) shift to lower frequencies. The relative values of the elements of the Raman tensors of the A_1 and E modes have been determined, and the Y^- halogen impurity is found to have a stronger influence on the E-mode tensor than on the A_1-mode tensor. A calculation of these elements within the framework of the valence optical theory provides an understanding of their behavior. A localized vibration of the doubly perturbed H_i^0 defect, the $H_i^0(Y^-Y^-)$ center, is also detected at still lower energies and is shown to belong to the B_2 representation of the point group $C_{2v}[001](110,1\bar{1}0)$. The relationships between the mode frequencies of the various H_i^0-type centers are discussed.

I. INTRODUCTION

The properties of localized modes of impurity defects in solids have been studied extensively by means of Raman scattering and infrared spectroscopy.[1] Recently, we have measured the inelastic light scattering of several radiation defects in alkali halides and have determined the frequency of their vibrational modes.[2–5] In the preceding paper[6] a detailed discussion is given of a method which allows determination of the symmetry properties of a defect and its vibrational modes from the intensities of polarized Raman scattering of preferentially or randomly oriented defects. Any possible defect symmetry as well as any possible symmetry of the preferential orientation process, compatible with a cubic crystal structure, has been considered. The results, which are helpful in the application of the method, are summarized in a set of tables given in Ref. 6. In the present paper this method is applied to a Raman study of interstitial hydrogen atom (H_i^0) centers in alkali halides (A^+X^-) perturbed by substitutional halogen impurities Y^-, heavier than the host halogen ions X^-.

The properties of the H_i^0 centers, also called U_2 centers, have been extensively investigated by means of optical-absorption spectroscopy,[7–11] electron spin resonance[8,12,13] (ESR), electron-nuclear double resonance,[12–15] and Raman scattering.[4,5] The model of the center, which possesses T_d symmetry, is shown in Fig. 1(a). From Raman experiments it was determined that the threefold-degenerate T_2 mode of the defect is well described by the vibration of the H_i^0 atom in a quasistatic cage formed by the eight nearest-neighbor (NN) ions. In alkali halides doped with the heavier halogen impurities Y^-, it is possible to stabilize the interstitial hydrogen atom in a NN po-

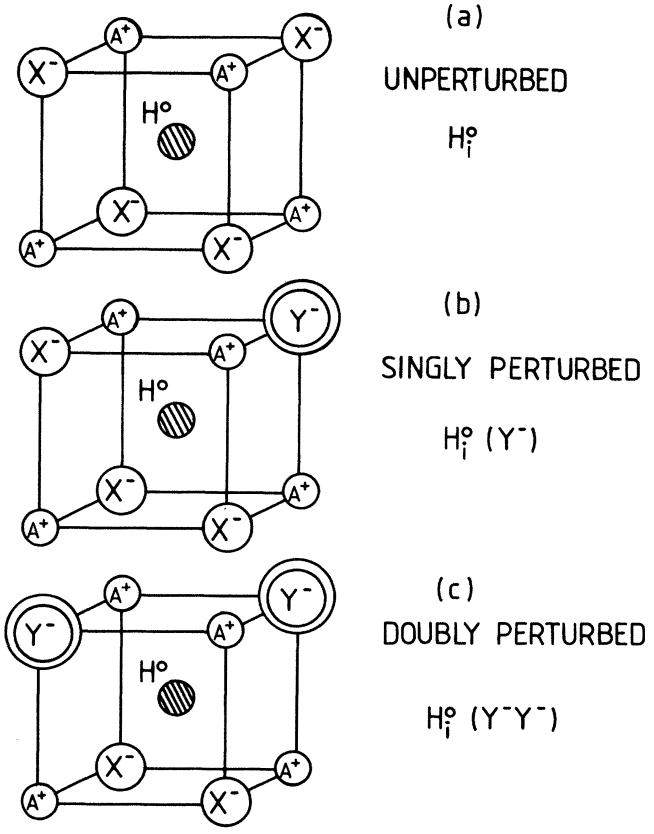

FIG. 1. Schematic models showing the unperturbed and perturbed interstitial hydrogen atom centers H_i^0, $H_i^0(Y^-)$, and $H_i^0(Y^-Y^-)$. The host anion and cation are indicated by X^- and A^+, and the impurity halogen anion by Y^-.

sition to such an impurity and to produce the singly perturbed H_i^0 center denoted by $H_i^0(Y^-)$ [see Fig. 1(b)]. The $H_i^0(Y^-)$ center was studied in a series of crystals by optical absorption[10,16] and ESR.[17] This defect possesses C_{3v} symmetry around the $\langle 111 \rangle$ axis connecting the H_i^0 atom and the Y^- impurity ion. The T_2 mode of the H_i^0 center is expected to be split by the perturbation into a A_1 vibration in which the H_i^0 atom moves along the threefold axis, and into a twofold-degenerate E mode in which the interstitial H_i^0 atom moves perpendicular to this axis. In this work (Secs. III and IV) we have identified and investigated the Raman scattering from the A_1 and E modes of the $H_i^0(Y^-)$ centers in a series of six crystals, i.e., RbCl:I^-, RbBr:I^-, KCl:I^-, KBr:I^-, RbCl:Br^-, and KCl:Br^-. The Raman tensors of the localized modes have been determined and they are compared to the Raman tensors of the T_2 mode of the unperturbed H_i^0 center (Sec. V).

Moreover, it has been possible to identify the Raman scattering of a doubly perturbed H_i^0 center, the so-called $H_i^0(Y^-Y^-)$ defect, which was found to possess $C_{2v}[100](011,0\bar{1}1)$ symmetry (Secs. III and IV). The proposed model of this defect is given in Fig. 1(c). The existence of such a doubly perturbed H_i^0 center was already reported by Fisher[10] on the basis of optical-absorption experiments, and also in an ESR study of the $H_i^0(Y^-)$ defects.[17]

In alkali-halide crystals doped with a cation impurity B^+, smaller than the host alkali ion, especially in KCl:Li^+ (Refs. 18 and 19) and KCl:Ag^+ (Ref. 19), it is possible to produce other types of perturbed H_i^0 defects. The polarized Raman scattering of H^0-Li^+ in KCl has been investigated in our laboratory and the results will be published in a planned forthcoming paper.[20]

II. EXPERIMENTAL PROCEDURES

The inelastic light scattering was measured with a Spex Raman instrument featuring a double monochromator and a photon counting system. A Kr^+-ion laser (Spectra Physics 171) tuned at a wavelength of 530.9 nm and run at a power of about 600 mW was employed as an exciting source. The crystals were mounted in a helium-cooled optical cryostat which permitted measurements of both Raman and optical-absorption spectra at each stage of the experiment. Special care was taken to obtain a good calibration of the optics in the Raman instrument and a high accuracy of the orientation of the crystal with respect to the polarization directions of the incident and scattered light.

The alkali-halide crystals used in our experiments were doped with heavier halogen impurities Y^- and with OH^- ions. The concentrations in the melt varied from 0.5 to 5 mol % for the Y^- ions, and from 0.1 to 0.2 mol % for the OH^- impurities.

The unperturbed H_i^0 centers were produced by uv irradiation from a deuterium lamp of the crystals at low temperature ($T \approx 15$ K) as described in Ref. 4. The singly perturbed $H_i^0(Y^-)$ were produced by a subsequent thermal anneal to temperatures between 75 and 100 K, depending on the crystal. In this temperature range the interstitial H_i^0 atom migrates through the crystal and it can be stabilized next to a substitutional Y^- halogen impurity ion.

Preferential bleaching of the defects in different orientations was achieved by polarized uv light (see Fig. 2) $T \approx 15$ K. The uv light was exciting the lowest-energy absorption band of the $H_i^0(Y^-)$ defect, e.g., the 320-nm I_1 or the 267-nm Br_1 band in RbCl according to the nomenclature of Ref. 16. The uv light originated from a deuterium light source, and was filtered by a Nicol prism polarizer and suitable cutoff filters. The polarized optical absorption of the crystals was measured with a double-beam spectrophotometer (Cary 17). A Nicol prism polarizer was inserted in the optical path before the splitting into a reference and a measuring beam: As a result compensation for the absorption by the polarizer was not necessary.

III. EXPERIMENTAL RESULTS

A. Production of the defects and correlation with the Raman measurements

In each of the crystals the production sequence described in Sec. II was followed. In Fig. 3 the resulting Raman spectra in RbCl doped with 2 mol % I^- are shown for four different optical geometry pairs[6] (OGP's): The scattering intensities are indicated by $I_{\alpha,\beta}$ in which the OGP (α,β) indicates the polarization directions of the incident and of the scattered light, respectively. The reference axes in which the directions are expressed are defined in Fig. 2. After the low-temperature uv irradiation the Raman peak of the unperturbed H_i^0 center is found[4] at 398 cm^{-1} as shown in Figs. 3(a) and 3(b). After a thermal anneal of the crystal at about 95 K for 5 min the intensity of the H_i^0 peak is strongly diminished and three new Raman peaks are observed [see Figs. 3(c) and 3(d)]. Figures 4 and 5 show the Raman spectra of the same crystal but for different OGP's. Through a parallel optical-absorption measurement it was confirmed that the perturbed $H_i^0(I^-)$ center, monitored at its I_1 band at 320 nm,[16] had been produced at the expense of the unperturbed H_i^0, monitored at 235 nm.

Subsequently, a $[0\bar{1}1]$ polarized uv bleach in the I_1 band of the $H_i^0(I^-)$ defect was performed at low temperature for about 200 min. By this treatment the concentration of the unperturbed H_i^0 defect grows again to about half of its

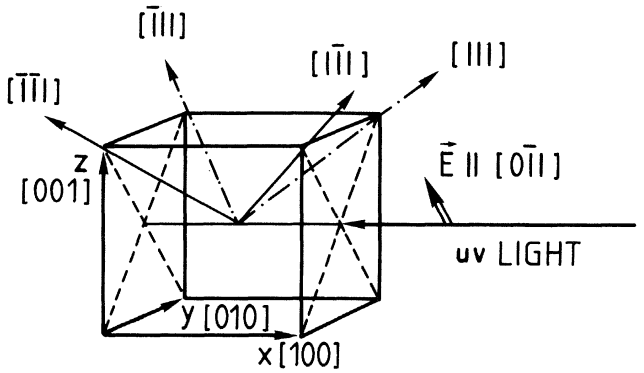

FIG. 2. Geometry of the bleaching direction of the polarized uv light and definition of the crystal reference frame (x,y,z).

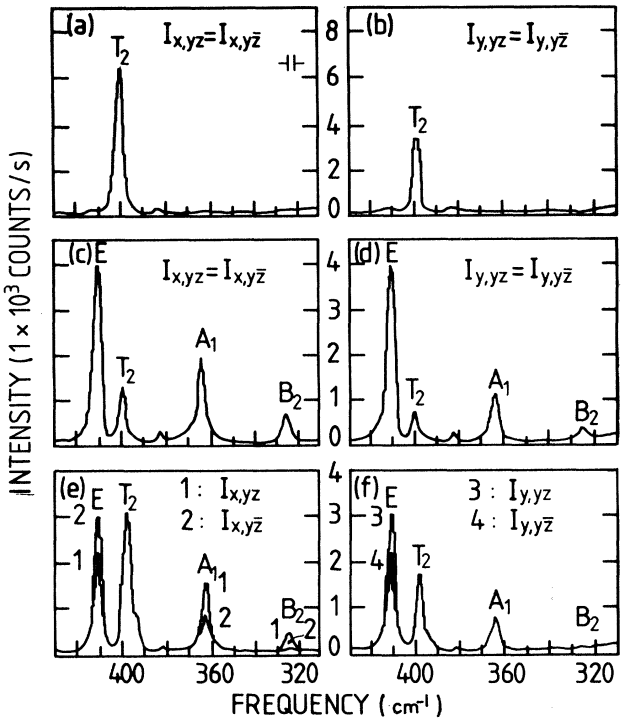

FIG. 3. Raman spectra of the H_i^0, $H_i^0(I^-)$, and $H_i^0(I^-I^-)$ centers in RbCl:I^- for several OGP's: (x,yz), $(x,y\bar{z})$, (y,yz), and $(y,y\bar{z})$, i.e., set 1.2 of Table II. Spectra (a) and (b) were measured after the unperturbed H_i^0 center was produced. Spectra (c) and (d) show that after a thermal anneal at 95 K ($F_1=T$) the Raman intensities of the C_{3v}:E and A_1 modes of $H_i^0(I^-)$ and the C_{2v}:B_2 mode of $H_i^0(I^-I^-)$ have grown at the expense of the mode T_2 of the unperturbed H_i^0 center. Spectra (e) and (f) were measured after a $[0\bar{1}1]$ polarized uv bleaching ($F_1=D_2[011]$) into the I_1 absorption band of the perturbed $H_i^0(Y^-)$ center. This bleaching has regenerated some unperturbed H_i^0 as evidenced by the increased T_2 mode.

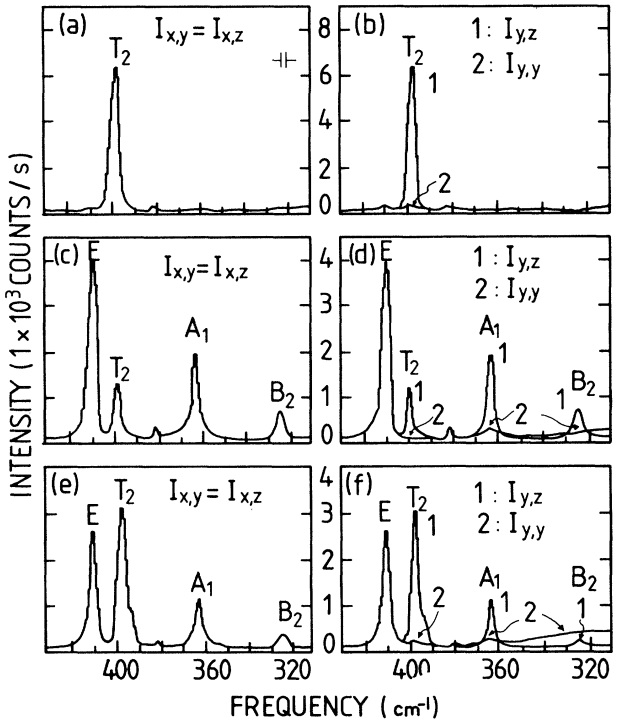

FIG. 4. Similar polarized Raman spectra as Fig. 3, but for OGP (x,y), (x,z), (y,z), and (y,y), i.e., set 1.1 of Table II.

original value, as is also seen in Figs. 3(e) and 3(f).

The intensities of the polarized Raman spectra $I_{\alpha,yz}$ and $I_{\alpha,y\bar{z}}$, with $\alpha=x$ or y, which in the previous spectra had been accurately equal, are shown in these figures to be unequal for the three new Raman peaks, but still equal for the unperturbed H_i^0 peak. This demonstrates that the defects from which the three new peaks originate are anisotropic and possess an absorption band in the region above the characteristic wavelength of the cutoff filter, $\lambda=305$ nm, in this experiment. The I_1 optical-absorption band of the $H_i^0(I^-)$ center, at 320 nm, which is a charge-transfer transition from the H^0 atom to the I^- ion,[16] is found at this stage to be strongly polarized indicating that about 40% of the centers with symmetry axes along $[1\bar{1}1]$ and $[11\bar{1}]$ have been preferentially destroyed by the polarized bleaching. In this bleaching process the interstitial H_i^0 atoms have moved back into an unperturbed interstitial

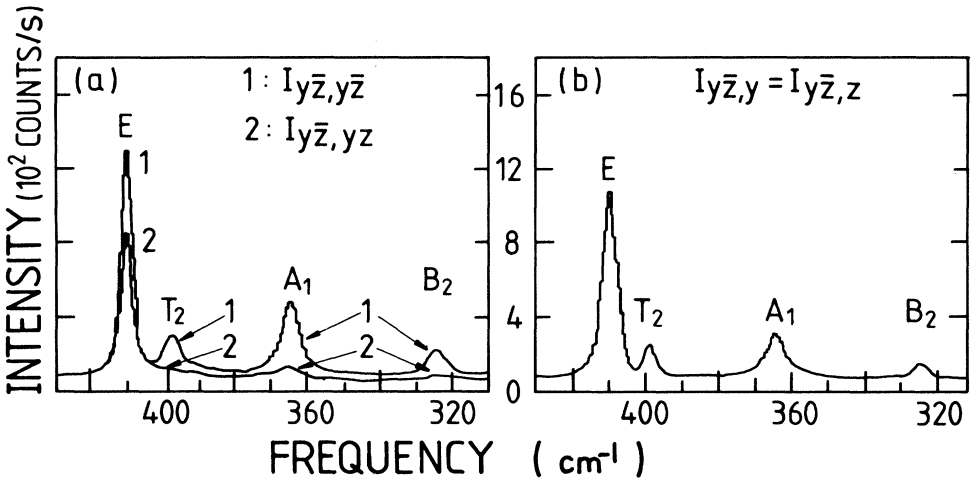

FIG. 5. Similar polarized Raman spectra as Figs. 3(c) and 3(d), but for the OGP $(y\bar{z},y\bar{z})$, $(y\bar{z},yz)$, $(y\bar{z},y)$, and $(y\bar{z},z)$, i.e., set 3.2 of Table II. The spectra were measured after an anneal of the sample at 95 K.

position, and this explains the partial recovery of the normal H_i^0 centers mentioned above.

The following facts strongly support the hypothesis that the new Raman peaks originate from a H_i^0 defect perturbed by an I^- impurity: (i) They cannot be produced in crystals without I^- doping, (ii) they possess a frequency in the neighborhood of the H_i^0 vibrational frequency, and (iii) they appear after the thermal anneal during which the H_i^0 atom can migrate through the crystal. It will be shown in Sec. IV C 1 that two of the peaks, i.e., those at 363 and 409 cm^{-1} in RbCl:I^- originate from the A_1 and the E modes of the $H_i^0(I^-)$ center, respectively. In each of the crystals the analogous Raman signals have been measured and the peak positions are listed in Table I together with the corresponding vibrational frequency of the H_i^0 defect. In three of the crystals, i.e., RbCl:Br^-, KCl:Br^-, and KCl:I^- the quantitative analysis of the Raman spectra was complicated by the fact that the E mode of the singly perturbed $H_i^0(Y^-)$ defect and the T_2 mode of the unperturbed H_i^0 defect overlap (see Table I). The differences in vibrational frequencies of the modes of $H_i^0(Y^-)$ center and the T_2 mode of the unperturbed H_i^0 center are also listed in Table I and show a systematic variation from one crystal to another.

The remaining Raman peak, at 323 cm^{-1} in RbCl:I^-, is not correlated with $H_i^0(I^-)$ defect. Through a comparison of measurements on RbCl:I^- samples with an iodine doping concentration of 0.5 and 2 mol%, it was found that this signal is, relative to the $H_i^0(I^-)$ signals, much stronger in the crystal with a higher I^- doping level. Therefore, this peak is believed to be associated with a H_i^0 interstitial stabilized next to a pair of substitutional I^- impurities (Sec. IV C 2). A similar Raman peak was observed in four of the crystals under study, and the corresponding frequencies are also listed in Table I. The proposed model of this center, which will be further called the doubly perturbed center $H_i^0(Y^-Y^-)$, is shown in Fig. 1(c) and consists of a H_i^0 interstitial flanked by two Y^- impurities in NN substitutional positions. Such a defect possesses $C_{2v}[001](110,1\bar{1}0)$ symmetry. The short notation $C_{2v}(110)$ will be employed from here on. From polarized Raman measurements it will be further argued (Sec. IV C 2.) that the Raman peak originates from the B_2 mode of this defect. In such a mode the interstitial H_i^0 vibrates parallel to the line joining the two Y^- impurities. Although the identification of the Raman peaks as given above will not be fully confirmed until Sec. IV C, we will already use this nomenclature for the vibrational modes under study.

B. Pulse-anneal experiments

In order to confirm the identification of the Raman spectra the following pulse-annealing experiments were performed: After the production of the unperturbed H_i^0 centers the crystal was warmed up for about 5 min to a temperature at which the interstitial H_i^0 atom becomes mobile. This was repeated using consecutively higher annealing temperatures with intervals of 5 K, and after each sequence the Raman spectra were measured at about 15 K. In Figs. 6 and 7 the intensities of the four Raman peaks are plotted as a function of the annealing temperature for the crystals RbCl:I^- and RbBr:I^-, respectively. Each of the curves is normalized to its maximum value.

The A_1 and E peaks of the $H_i^0(I^-)$ center follow very accurately the same thermal-anneal curve, which is distinctly different from the behavior of the H_i^0 and the $H_i^0(I^-I^-)$ peaks. This confirms that these two lines originate from the same defect. Moreover, in RbCl:I^- the height of the I_1 absorption peak of the $H_i^0(I^-)$ defect was also measured, and it shows qualitatively the same dependence on the annealing temperature as the Raman data (see Fig. 6). The small discrepancies are probably related to the fact that the $H_i^0(Y^-Y^-)$ absorption band overlaps the I_1 band.

The unperturbed H_i^0 signal, which decays during the conversion to $H_i^0(I^-)$, has a more complicated behavior showing a small recovery around 105 and 90 K for RbCl:I^- and RbBr:I^-, respectively. The $H_i^0(I^-I^-)$ peak grows at a somewhat higher temperature than the $H_i^0(I^-)$ signals, and possesses a slightly higher decay temperature also. The center seems to form a somewhat deeper trap for the interstitial H_i^0 atom than the $H_i^0(I^-)$ defect.

In the remaining crystals the same experiment was attempted but without conclusive results: Either the depen-

TABLE I. Vibrational frequencies (in cm^{-1}) of the interstitial hydrogen atom in the unperturbed H_i^0 centers and in the singly or doubly perturbed $H_i^0(Y^-)$ and $H_i^0(Y^-Y^-)$ centers in various alkali halides, and the inhomogeneous linewidth (in cm^{-1}) of these Raman peaks. The difference in vibrational frequencies between the modes of the H_i^0 and of the $H_i^0(Y^-)$ or $H_i^0(Y^-Y^-)$ centers are also listed. All frequencies are accurate to about 1 cm^{-1}.

	Frequency				*Differences*			*Linewidth*			
	H_i^0	$H_i^0(Y^-)$		$H_i^0(Y^-Y^-)$				H_i^0	$H_i^0(Y^-)$		$H_i^0(Y^-Y^-)$
Crystal	T_2	E	A_1	B_2	E–T_2	A_1–T_2	B_2–T_2	T_2	E	A_1	B_2
RbCl:2%I^-	398	409	363	323	11	−35	−75	1.3(1.0)[b]	2.3(1.2)[b]	2.6(1.4)[b]	3.2
KCl:1%I^-	439	439[a]	418	–	0[a]	−21	–	1.6	1.6	1.8	–
RbBr:5%I^-	330	345	284	269	15	−46	−61	10	9	10	13
KBr:5%I^-	366	372	335	320	6	−31	−46	7	9	9	10
RbCl:1%Br^-	398	398[a]	375	–	0[a]	−23	–	–	–	–	–
KCl:5%Br^-	437	437[a]	421	415	0[a]	−16	−22	7	7	7	–

[a]The errors are roughly equal to half of the corresponding inhomogeneously broadened peak widths because of overlap of the T_2 and E modes, i.e., about 1 cm^{-1} for KCl:I^- and RbCl:Br^-, and about 3.5 cm^{-1} for KCl:Br^-.

[b]The linewidth values between parentheses are for RbCl:0.5%I^-

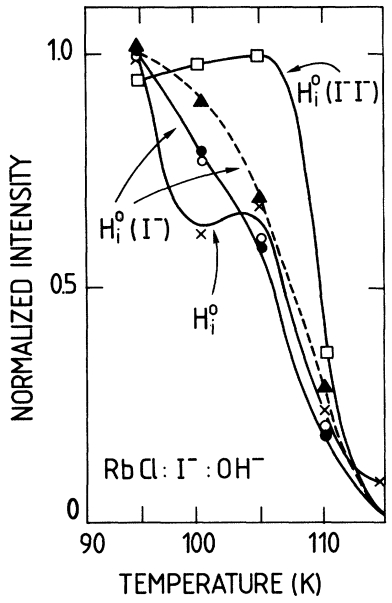

FIG. 6. Normalized intensities of the pulse-anneal curves in RbCl:I^-. The dashed line indicates the behavior of the optical density of the $H_i^0(I^-)$ center I_1 band at 320 nm; the solid lines indicate Raman intensities. The E and A_1 modes of the $H_i^0(I^-)$ are indicated by ● and ○, respectively, the B_2 mode of $H_i^0(I^-I^-)$ is indicated by □, and the T_2 mode of the unperturbed H_i^0 center is indicated by ×.

dence of the peak intensities on the annealing temperature was too difficult to determine because of overlap between Raman peaks and because of a low signal level, or else the different peaks followed nearly the same dependence and no conclusions could be drawn.

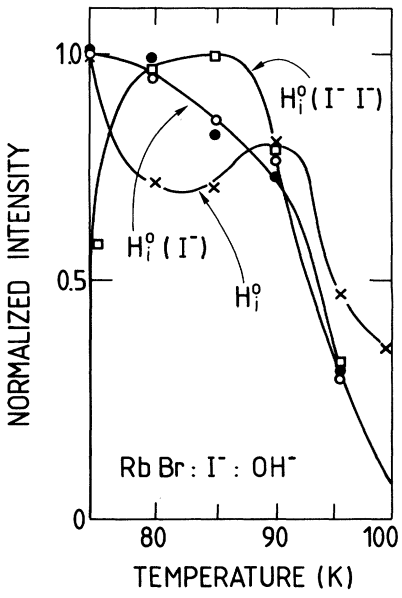

FIG. 7. Similar pulse-anneal results as in Fig. 6 but for RbBr:I^-. The symbols follow Fig. 6 except that there are no pulse-anneal data on optical absorption.

IV. ANALYSIS OF THE POLARIZED RAMAN SPECTRA

A. Behavior-type analysis method

The method applied for the analysis of the Raman spectra is discussed in detail in the accompanying paper[6] and only its essential features will be summarized here. The intensity I of the Raman scattering of a vibrational mode of a defect can be written as

$$I = kI_0 \sum_{i,j,i',j'} a_i b_j a_{i'} b_{j'} P_{iji'j'} , \tag{1}$$

in which the a_i and b_j are the components of the polarization vectors (with respect to the lattice coordinates x, y, and z, see Ref. 6) of the incident and scattered light, respectively, I_0 is the intensity of the incident laser beam, k is an instrumental efficiency factor, and $P_{iji'j'}$ is a so-called intensity parameter (IP). A pair of polarization vectors $(\vec{a},\vec{b})$ is an OGP. There are 21 independent IP's containing all of the information that can be derived from Raman scattering about the vibrational mode of the defect. The IP's are given by

$$P_{iji'j'} = \sum_n N_n T_{ij}^{(n)} T_{i'j'}^{(n)} , \tag{2}$$

where N_n is the population number of the nth orientation of the defect and $T_{ij}^{(n)}$ is a component of the Raman tensor of the vibrational mode of a defect in this orientation. For the sake of brevity the 21 IP's have been given a short notation, q_i, r_i, s_i, t_i, u_i, and v_j with $i=1,2,3$, and $j=1,\ldots,6$ [see Eqs. (8) of Ref. 6]. It is often possible to influence the population numbers N_n by a physical process (e.g., by polarized light) which is described by an orientating operator $\hat{F}$. As is discussed in Ref. 6 it is not necessary to consider the actual symmetry groups of the defects and of the operator $\hat{F}$, which are subgroups of the point group O_h, but it is sufficient to work with the so-called *representative symmetry* groups, O_1 and F_1, which are subgroups of the smaller cubic point group O, because the Raman tensor is invariant under inversion symmetry. The possible modes of the defects have been classified in 25 sets of modes, the so-called *representative modes,* which are the only ones that can possibly be distinguished by polaized Raman measurements.

For a given representative mode and a given symmetry F_1 the number of independent IP's is often reduced: Some of the IP's become zero, or simple specific relations exist among the IP's. The set of these IP relations [Eqs. (18) and Table VII in Ref. 6] defines the so-called *behavior type* (BT) of the IP. The BT's have been investigated for any possible representative symmetry $F_1 \subset O$ of the orientating operator $\hat{F}$ and any possible representative mode of the defects. The basic idea of the method is to determine the BT from the experimental Raman intensity data, and in this way to determine the representative defect symmetry O_1 and the representative modes, instead of directly trying to determine the Raman-tensor elements and the population numbers N_n from Eqs. (1) and (2) which are difficult to solve. Once the symmetry properties of the defect and its vibrational modes are determined it is often

TABLE II. Raman scattering intensities $I_{\alpha,\beta}$ expressed as a function of the IP's for two representative symmetries, F_1 of the orientating operator $\hat{F}$. The corresponding order e of the angular errors are also listed. This table is simplified from Table XI of Ref. 6.

Optical geometry	$F_1 = D_2[011]$	e	$F_1 = T$	e
Set 1.1	$I_{x,y} = s_2$	1	$I_{x,y} = s$	2
	$I_{x,z} = s_2$	1	$I_{x,z} = s$	2
	$I_{y,z} = s_1$	2	$I_{y,z} = s$	2
	$I_{y,y} = q_2$	1	$I_{y,y} = q$	2
Set 1.2	$I_{y,yz} = \frac{1}{2}(s_1 + q_2 + 2v_1)$	1	$I_{y,yz} = \frac{1}{2}(s+q)$	1
	$I_{y,y\bar{z}} = \frac{1}{2}(s_1 + q_2 - 2v_1)$	1	$I_{y,y\bar{z}} = \frac{1}{2}(s+q)$	1
	$I_{x,y\bar{z}} = s_2 - t_1$	2	$I_{x,y\bar{z}} = s$	2
	$I_{x,yz} = s_2 + t_1$	2	$I_{x,yz} = s$	2
Set 3.2			$I_{x,yz} = s$	2
			$I_{x,y\bar{z}} = s$	2
			$I_{y\bar{z},y\bar{z}} = \frac{1}{2}(q+r) + s$	2
			$I_{y\bar{z},yz} = \frac{1}{2}(q-r)$	2

possible to simplify the IP expressions [Eq. (2)] substantially.

In Table II the Raman scattering intensities which could be measured in our experiments are listed as a function of the IP for the representative symmetries F_1 of the orientating operator $\hat{F}$ employed in the experiment: The uv bleaching polarized along $[0\bar{1}1]$ (see Sec. II and Fig. 2) yields the symmetry $F_1 = D_2[011]$, while randomly oriented defects correspond to the symmetry O_h of the operator $\hat{F}$, i.e., a representative symmetry $F_1 = T$. Table II is extracted from Table XI in Ref. 6. The lower index of the IP is omitted if the IP is independent of this index, e.g., s stands for $s_1 = s_2 = s_3$. The OGP's have been classified into sets which can be experimentally realized without rotating the sample. In our experiments only set 1 was employed[6] for the preferentially orientated defects, $F_1 = D_2[011]$, and both sets 1 and 3 are applied to the randomly oriented defects, $F_1 = T$.

The BT which can occur for the symmetries $F_1 = D_2[011]$ and $F_1 = T$ are listed in Table III for each of the possible representative modes. No optical anisotropy was produced with $F_1 = D_4[100]$ light and consequently these BT's are not listed in Table III. Only that part of the BT relations is listed that can be verified on the basis of our measurements (see Sec. IV C 1), in which for OGP set 1 and $F_1 = D_2[011]$ we could measure five IP's and for OGP set 3 with $F_1 = T$ we could measure three IP's. Table III is derived from Tables VII and VIII in Ref. 6, and it is instructive to investigate it.

As discussed in Ref. 6 it is possible that the experimen-

TABLE III. BT's and corresponding sets of representative modes that must be considered on the basis of five measured Raman IP's obtained in (OGP) set 1 with orientating operator $F_1 = D_2[011]$, and three IP's obtained in OGP set 3 with $F_1 = T$. This table is extracted from Tables VII and VIII of Ref. 6.

Sets of distinguishable Representative modes	OGP Set 1 $F_1 = D_2[011]$	OGP Set 3 $F_1 = T$
1 C_1:A, $C_2[110]$:A	$q_2\ s_1\ s_2\ t_1\ v_1$	$q\ r\ s$
2 $C_2[010]$:A, $D_2[110]$:A	$q_2\ s_1\ s_2\ 0\ v_1$	$q\ r\ s$
3 $C_2[010]$:B, $D_2[110]$:B_2,B_3	$0\ s_1\ s_2\ t_1\ 0$	$0\ 0\ s$
4 $C_2[110]$:B	$q_2\ s_1\ s_2\ t_1\ v_1$	$q\ -\frac{1}{2}q\ s$
5 $D_2[100]$:A, $C_4[001]$:A, $D_4[001]$:A_1	$q_2\ 0\ 0\ 0\ 0$	$q\ r\ 0$
6 $D_2[100]$:B_1, $C_4[001]$:E, $D_4[001]$:B_2,E	$0\ s_1\ s_2\ 0\ 0$	$0\ 0\ s$
7 $D_2[110]$:B_1, $D_4[001]$:B_1, T:E	$q_2\ 0\ 0\ 0\ 0$	$q\ -\frac{1}{2}q\ 0$
8 $C_3[111]$:A, $D_3[111]$:A_1	$q\ s\ s\ t_1\ v_1\ \lvert v_1/t_1\rvert = (q/s)^{\frac{1}{2}}$	$q\ q\ s$
9 $C_3[111]$:E	$q\ s\ s\ t_1\ v_1$	$q\ -\frac{1}{2}q\ s$
10 $D_3[111]$:E	$q\ s\ s\ t_1\ v_1\ \lvert v_1/t_1\rvert = (q/s)^{\frac{1}{2}}$	$q\ -\frac{1}{2}q\ s$
11 $C_4[001]$:B	$q_2\ s_1\ s_2\ 0\ 0$	$q\ -\frac{1}{2}q\ s$
12 T:A	$q\ 0\ 0\ 0\ 0$	$q\ q\ 0$
13 T:T	$0\ s\ s\ 0\ 0$	$0\ 0\ s$

tally measured IP's of a vibrational mode obey the BT relations accidentally, i.e., for reasons other than symmetry arguments. A so-called *observed* BT is thus measured corresponding to a higher symmetry than that of the actual vibrational modes. Therefore, one must check all of the so-called *actual* BT's, i.e., the BT derived purely from symmetry arguments, which can correspond to this observed BT.

B. Evaluation of the experimental errors

We have carefully evaluated the experimental errors on the measured Raman intensities taking into account the statistical errors on the number of photon counts, and the accidental errors due to slight misalignments of the crystal or of the optical assembly. In Table II the error order e is indicated for the intensity error ΔI as a function of angle deviations $\Delta\beta_i$ of the crystal orientation: $\Delta I \sim (\Delta\beta)^e$. The accidental errors were monitored by taking the signals of the unperturbed H_i^0 defect as an indicator and checking a number of OGP's with theoretically equal Raman intensities (see Table XIV in Ref. 6). In fact, the sample orientation was improved on the basis of these monitoring measurements. The relative accidental errors on the final measurements are estimated to be about ±2.5%.

It should also be noted that while the preferentially bleached (with $F_1 = D_2[011]$) perturbed H_i^0 centers were being measured, a slow reorientation induced by the laser beam was observed (530.9 nm, 100–800 mW). The reorientation rates are quite slow and are different in different crystals. Using polarized light optical absorption we have measured the ratio $d_{[0\bar{1}1]}/d_{[011]} = N_2/N_1$ before and after the Raman measurements. The mean value and the difference were taken as the experimental value of $d_{[0\bar{1}1]}/d_{[011]}$ and its error, respectively (Table IV).

C. Behavior-type analysis of the H_i^0-type Raman spectra

The results of the polarized Raman measurements on the perturbed H_i^0 centers as derived from spectra of the types measured in Figs. 3–5 are summarized in Table IV, both for the preferentially ($F_1 = D_2[011]$) and for the randomly ($F_1 = T$) orientated defects. In RbCl:I^- it was possible to produce a relatively high concentration of the two perturbed H_i^0 centers in a sample with a relatively low halogen impurity concentration (≈2 mol %). As a result the data in RbCl:I^- possess the highest precision and reliability compared to the other samples, and we will first discuss the measurements in this crystal. We will comment on specific features which occur in the other crystals later.

1. Analysis of the $H_i^0(Y^-)$ spectra

By making use of the relations which define the BT (Table III) it was possible to definitely eliminate a number of possible representative modes on the basis of the following experimental results which are found for the E peak of the $H_i^0(I^-)$ spectrum in the RbCl:I^- sample. For $F_1 = D_2[011]$,

$$q_2, s_1, s_2, t_1, v_1 \neq 0 \,, \tag{3a}$$

and for $F_1 = T$,

$$q, r, s \neq 0 \,, \quad r/q \neq 1 \,. \tag{3b}$$

TABLE IV. Relative values of the IP's obtained from the experimental Raman intensities, and the values $d_{[01\bar{1}]}/d_{[011]}$ obtained from polarized optical absorption are given for the A_1 and E peaks of the $H_i^0(Y^-)$ center. The IP ratios for the B_2 peak of the $H_i^0(Y^-Y^-)$ center are also listed.

		$F_1 = D_2[011]$						$F_1 = T$	
Crystal	Mode	q_2/s_2	s_1/s_2	t_1/s_2[a]	v_1/s_2	v_1/t_1[b]	$d_{[01\bar{1}]}/d_{[011]}$	q/s	r/q
RbCl:	E	0.98±.07	0.95±.07	−0.17±.05(−0.13±.06)	0.20±.05	−1.3±.4(0.99±.04)	0.6±.1	0.9±.1	−0.6±.1
2%I^-	A_1	0.08±.03	0.97±.09	0.32±.06(0.3±.1)	0.05±.04	0.15±.12(0.28±.05)		0.07±.02	–
	B_2	0.0±.2	0.5±.2	0.6±.2	0.0±.2	0.0±.3		0.05±.04	–
KCl:	E	1.1[c]	1.00±.08	−0.17[c](−0.18±.02)	0.15[c]	0±3(1.1[c])	0.47±.03	0.41±.04[d]	−0.5±.3
1%I^-	A_1	0.00±.06	1.0±.1	0.32±.08(0.37±.05)	0.00±.06	0.0±.2(0.27±.09)		0.08±.05	–
RbBr:	E	–	–	−0.24±.07(−0.23±.06)	0.17±.09	−0.8±.5(0.73±.04)	0.4±.1	0.53±.06	–
5%I^-	A_1	–	–	0.5±.1(0.5±.1)	0.2±.1	0.31±.25(0.33±.07)		0.11±.05	–
	B_2	–	–	0.5±.1	0.0±.15	0.0±.3		0.12±.04	–
KBr:	E	–	–	−0.36±.09(−0.39±.03)	0.23±.07	−0.7±.3(0.67±.04)	0.13±.02	0.45±.05	–
5%I^-	A_1	–	–	0.8±.1(0.77±.05)	0.10±.07	0.12±.08(0.0±.2)		0.00±.03	–
	B_2	–	–	0.6±.2	0.0±.1	0.0±.2		0.16±.08	–
RbCl:	E	0.14[c]	1.02±.08	−0.41[c](∼ −0.4)	0.03[c]	0.0±.3(0.37[c])	∼0.1	0.05±.01[d]	–
1%Br^-	A_1	0.4±.3	1.0±.4	0.5±.3(∼0.9)	0.0±.2	0.0±.6(0.4±.1)		0.14±.07	–
KCl:	E	0.24[c]	0.97±.07	−0.38[c](−0.42±.08)	0.12[c]	−0.5±.5(0.49[c])	0.09±.01	0.06±.02[d]	–
5%Br^-	A_1	0.08±.06	1.0±.1	0.8±.1(0.8±.2)	0.18±.07	0.2±.1(0.3±.1)		0.07±.04	–

[a]The values inside the parentheses are calculated from the polarized optical absorption data by Eqs. (4a) and (4b) (see Table V and Sec. IV.C.1).

[b]The values between parentheses are calculated from $(q/s)^{1/2} = |v_1/t_1|$ for C_{3v} symmetry (see Table III and Sec. IV.C.1).

[c]In these crystals the E mode of $H_i^0(Y^-)$ center overlaps the T_2 mode of the H_i^0 center. The values are estimated by subtracting the Raman intensity of the H_i^0 center. The amount of H_i^0 center is used as a fitting parameter.

[d]These values are not corrected for overlap of the T_2 and E peaks.

Only four out of the thirteen BT's listed in Table III are consistent with these results (Nos. 1, 4, 9, and 10) and one of them, namely No. 10, corresponds to the representative mode $D_3[111]$:E which includes the E mode of the $H_i^0(I^-)$ defect with $C_{3v}[111]$ symmetry.

In order to further narrow down the representative mode it is useful to check other BT relations. The experimental data (Table IV) are found to obey very closely the following rules for $F_1=D_2[011]$:

$$s_1/s_2=1 ,$$

and for $F_1=T$,

$$r/q=-\tfrac{1}{2} .$$

These rules are only found for the E modes in the $C_3[111]$ and $D_3[111]$ representative symmetries, i.e., Nos. 9 and 10 in Table III. Finally, within the experimental accuracy the additional BT relation (Table III) for $F_1=D_2[011]$

$$|v_1/t_1|=(q_2/s_2)^{1/2}=(q/s)^{1/2} \tag{3c}$$

is also obeyed as can be seen in Table IV. This BT only applies to the E mode of representative symmetry $D_3[111]$, i.e., No. 10 in Table III. In order to check this relation the values $(q_2/s_2)^{1/2}$ are listed between parentheses in the v_1/t_1 column of Table IV.

For the A_1 peak of the $H_i^0(I^-)$ spectrum the elimination procedure is somewhat less rigorous: Among the IP relations (3) only $t_1\neq 0$ for $F_1=D_2[011]$ and $s\neq 0$ for $F_1=T$ were unambiguously determined. This is consistent with six of the thirteen BT (Nos. 1, 3, 4, 8, 9, and 10 in Table III). However, the relation $s_1/s_2=1$ is very accurately obeyed (see Table IV) and this only occurs for the representative modes of $C_3[111]$ and $D_3[111]$ (Nos. 8–10 in Table III). Taking also into account the results of the production and pulse-anneal experiments (Sec. III) which show that the two modes measured in the experiment belong to the same defect, we conclude that we are dealing with a defect possessing a representative symmetry $D_3[111]$. We delay until the end of this section the argument leading to the actual C_{3v} symmetry of the $H_i^0(Y^-)$ center.

If only the Raman data concerning the A_1 mode were available and taking into account that q_2/s_2 and v_1/t_1 are very near to zero (see Table IV), the BT corresponding to the representative modes $C_2[010]$:B, and $D_2[110]$:B_2 and B_3 would have to be considered. However, the fact that q_2 and v_1 nearly vanish does not result from the symmetry properties of the mode, but reflects the fact that compared to the unperturbed H_i^0 center, the Raman tensor of the A_1 mode of the $H_i^0(I^-)$ center is not drastically influenced by the presence of the I^- impurity as will be discussed in Sec. V.

Characteristic relations between the IP's of different modes of the same defect were found to exist for several defect symmetries O_1: All of these relations are given in Table IX of Ref. 6. For the representative modes $D_3[111]$:E and A_1 the following constraints on the IP were found:

$$\left[\frac{t_1}{s_2}\right]_{A_1}=-2\left[\frac{t_1}{s_2}\right]_E=\frac{N_1-N_2}{N_1+N_2} , \tag{4a}$$

in which N_1 is the population number of the defect orientations with a threefold axis along [111] and $[\bar{1}11]$, while N_2 is that number for the $[1\bar{1}1]$ and $[11\bar{1}]$ orientations. The first part of Eq. (4a) is accurately obeyed for the A_1 and E peaks in RbCl:I^- (Table IV). According to the bleaching properties of the $H_i^0(I^-)$ center (Sec. III A) the relation $N_1>N_2$ must hold and hence $(t_1/s_2)_{A_1}>0$ as is indeed found in the experiment. Finally it is possible to determine the ratio N_2/N_1 from the polarized optical densities of the I_1 absorption band (see Sec. II): If d_α is this optical density for light polarized along the direction indicated by α then

$$N_2/N_1=d_{[0\bar{1}1]}/d_{[011]} . \tag{4b}$$

It should be kept in mind that the optical densities d_α are measured over the whole thickness of the crystal, in contrast to the Raman measurements in which only a small volume covered by the focused laser beam is involved, and that this could contribute to differences between the two types of data. The t_1/s_2 ratios derived from the polarized optical-absorption data [see Eq. (4)] are given between parentheses in Table IV together with the corresponding Raman results. One notes that they are in good agreement with each other.

The experimental results for the $H_i^0(Y^-)$ modes in the other crystals are very similar to those given above for RbCl:I^-. Owing to experimental circumstances the data are sometimes incomplete and less reliable than those for RbCl:I^-. The concentration of $H_i^0(Y^-)$ centers was lower in the other crystals, and as a result both the Raman and the optical-absorption signals were weaker. Higher experimental errors on the ratios of the IP resulted from this. As mentioned earlier (Sec. III A) in RbCl:Br^-, KCl:Br^-, and KCl:I^- the E peak of the $H_i^0(Y^-)$ spectrum overlaps with the T_2 peak of the unperturbed H_i^0 center. Therefore, the IP ratios q_2/s_2, t_1/s_2, and v_1/s_2 of the E modes could not be directly determined for $F_1=D_2[011]$. An attempt was made to subtract the contributions of the unperturbed H_i^0 defects: The relative amount of H_i^0 centers with respect to $H_i^0(Y^-)$ centers was used as a fitting parameter in order to obtain the set of IP's which is in the best agreement with the following relations [see Table III and Eqs. (4)]:

$$(t_1/s_2)_E=-\tfrac{1}{2}(t_1/s_2)_{A_1} ,$$

$$(t_1/s_2)_E=-\tfrac{1}{2}(N_1-N_2)/(N_1+N_2) .$$

The results of this procedure are listed in Table IV. The ratio q/s for $F_1=T$ given in Table IV for these three crystals could not be corrected for the overlap of the E and T_2 peaks. In the crystals with 5 mol% concentration of halogen impurities the Raman lines were found to exhibit an inhomogeneous broadening with a linewidth of about 7–10 cm^{-1}. This formed an additional source of errors due to overlap between different Raman peaks. Finally, in the measurements with OGP set 3 (see Tables I and IV) the crystals had to be ground and polished along a (110) plane. This procedure was only applied to the RbCl:I^- and KCl:I^- crystals.

So far our discussion has been based on the so-called[6] *observed* BT, i.e., the BT obeyed by the experimentally

determined IP. In Ref. 6 it was pointed out that the observed BT may accidentally possess a higher symmetry (i.e., more IP relations) than the *actual* BT of the center under consideration, and Table X of Ref. 6 lists the possible hierarchies. Consequently, we will redo the reasoning. The argument will be restarted from the point in the analysis where we concluded that the two Raman peaks induce the observed BT Nos. 8—10 in Table III. The notation of Ref. 6 will be used in the remainder of this section and the corresponding BT Nos. in Table VII of Ref. 6 are 21, 23a, and 23b, respectively. The corresponding sets of actual BT's are (16 21 24), (16 23a 41), and (16 23a 23b 41) as can be seen from Table X in Ref. 6. First we note that BT No. 16 is impossible because it does not occur in either the $F_1=D_2[011]$ or the $F_1=T$ column of Table VII in Ref. 6 and these were the only orientating symmetries used. Second, we know from the production and pulse-anneal data (Sec. III) that the two modes belong to the same center. This eliminates BT No. 41 because it is not paired with either BT Nos. 23a or 23b within a representative defect symmetry in Table VIII of Ref. 6 for any F_1 symmetry, $F_1=D_2[011]$ in particular. This leaves pairs Nos. 21,23a and Nos. 21,23b as the only possibilities, i.e., representative symmetries $C_3[111]$ and $D_3[111]$. The former representative symmetry represents the actual symmetries C_3 and S_6 and the latter one represents D_3, C_{3v}, and D_{3d} (Tables II and VI in Ref. 6). However, we can again eliminate $C_3[111]$ because relation (3c) is obeyed within experimental error. The last argument can be bypassed if one wishes by the following reasoning which uses a minimum of skeletal information about the center that were are investigating: The $H_i^0(Y^-)$ center possesses two constituent impurities (a hydrogen and a halogen), and it is impossible to construct with these in the alkali halides a defect possessing either C_3, S_6, D_3, or D_{3d} symmetry. As a result the $H_i^0(Y^-)$ center must possess C_{3v} symmetry. This of course we knew already but we have derived it from the Raman data using the BT analysis method.

2. *Raman spectrum of $H_i^0(Y^-Y^-)$ defects*

In an analogous way as for the $H_i^0(I^-)$ spectra in RbCl:I^- the number of possible BT's given in Table III can be reduced from thirteen to three (Nos. 1, 3, and 4 in Table III) for the $H_i^0(I^-I^-)$ peak in RbCl:I^- on the basis of the following experimentally determined IP relations for $F_1=D_2[011]$:

$$s_1,s_2,t_1\neq 0\ ,$$

$$s_1/s_2\neq 1\ .$$

The confirmation of the representative symmetry $O_1=D_2[110]$, which contains the defect symmetry $C_{2v}(110)$ of the proposed defect model (see Fig. 1c), is more hazardous if only the Raman measurements are considered. However, for $F_1=D_2[011]$ the following characteristic relations of the BT of the $D_2[110]$:B_2 and B_3 modes are obeyed within the experimental accuracy:

$$q_2,v_1=0\ ,$$

which is an argument in favor of the proposed $H_i^0(Y^-Y^-)$ model which possesses $C_{2v}(110)$ symmetry. One of the BT relations for $F_1=T$, namely

$$q=0$$

is not accurately obeyed in the experiment. The ratio q/s is quite small but, according to our analysis, it is different from zero (see Table IV). This is most likely caused by the overlap of the rather weak $H_i^0(I^-I^-)$ peak with Raman signals of a different origin. In such heavily doped crystals the occurrence of several H_i^0-type defects with structures close to our defects is to be expected. However, it is still possible, albeit unlikely, that the $H_i^0(Y^-Y^-)$ center possesses a lower symmetry, but even in that case it should be near the proposed $C_{2v}(110)$ symmetry.

We will further support the proposed model by combining, on the one hand, the Raman results, with, on the other hand, the expected properties of a $H_i^0(I^-I^-)$ defect preferentially bleached by $[0\bar{1}1]$ polarized uv radiation (see also Sec. II). Considering the model of Fig. 1(c) the $H_i^0(Y^-Y^-)$ defect can take six orientations. If the model in Fig. 1(c) is taken as the original orientation v_1, with the pair of Y^- ions parallel to [110], and following the notations of the accompanying paper,[6] these six orientations are v_1, v_3, v_9, v_{10}, v_{13}, and v_{14} (see Ref. 6: Tables I and the left cosets of the representative symmetry $D_2[110]$ in Table IV(b)) corresponding to the face diagonals [110], $[1\bar{1}0]$, [101], $[10\bar{1}]$, [011], and $[0\bar{1}1]$, respectively. Furthermore, taking the uv light polarized along $[0\bar{1}1]$ with a symmetry $F_1=D_2[011]$ the orientations v_1, v_3, v_9, and v_{10} possess the same bleaching rate, and as a result $N_1=N_3=N_9=N_{10}$ after the optical bleaching [see Table IV(a) in Ref. 6].

The $H_i^0(I^-I^-)$ defect is preferentially bleached very probably because it possesses an absorption band which overlaps the 320-nm I_1 band of the $H_i^0(I^-)$ center. If this absorption band is also caused by a charge-transfer transition from an I^- ion to the H^0 atom, similar to the I_1 absorption band, one expects a large absorption efficiency when the polarization vector of the uv light has a component along the H_i^0—I^- bond. As a result one expects for the $H_i^0(I^-I^-)$ defect nearly no bleaching for the orientation v_{13}, while v_{14} is expected to be bleached about twice as fast compared to the orientations v_1, v_3, v_9, and v_{10}.

In Table V the explicit expressions of the IP as a function of the Raman-tensor elements and of the population numbers are listed for the B_1 and B_2 modes in the defect symmetry $C_{2v}(110)$. These modes correspond to the representative modes $D_2[110]$:B_2 and B_3, respectively. From $N_{13}>N_{14}$ and the explicit expressions it follows that $(t_1/s_2)_{B_2}<0$ and $(t_1/s_2)_{B_2}>0$. The representative mode $D_2[110]$:B_2 is eliminated for the $H_i^0(I^-I^-)$ peak because in the experiment $t_1/s_2>0$ is found. From the explicit expressions in Table V it is also possible to derive the ratios of the population numbers as a function of the IP. Considering $D_2[110]$:B_3, and filling in the experimental values of the IP, one finds

$$\frac{N_1}{N_{13}}=\frac{s_1/s_2}{2-(s_1/s_2)+2(t_1/s_2)}\approx 0.19\ ,$$

$$\frac{N_{14}}{N_{13}}=\frac{2-(s_1/s_2)-2(t_1/s_2)}{2-(s_1/s_2)+2(t_1/s_2)}\approx 0.11\ , \tag{5}$$

TABLE V. IP's for two representative symmetries F_1 of the orientating operator $\hat{F}$, expressed as a function of the population numbers N_n and the Raman-tensor elements T_{ij} for the modes of the defect symmetries $C_{3v}[111]$:A_1 and E, and $C_{2v}(110)$:B_1 and B_2. This table is extracted from the Tables II—V, VII, and VIII of Ref. 6.

Vibrational mode	Representative mode	$F_1 = D_2[011]$	$F_1 = T$
$C_{3v}[111]$:A_1	$D_3[111]$:A_1	$q = 12kI_0(N_1+N_2)a'a'$ $s = 12kI_0(N_1+N_2)b'b'$ $t_1 = 12kI_0(N_1-N_2)b'b'$ $v_1 = 12kI_0(N_1-N_2)a'b'$	$q = 24kI_0N_1a'a'$ $s = 24kI_0N_1b'b'$
$C_{3v}[111]$:E	$D_3[111]$:E	$q = 24kI_0(N_1+N_2)d'd'$ $s = 24kI_0(N_1+N_2)e'e'$ $t_1 = 12kI_0(-N_1+N_2)e'e'$ $v_1 = 12kI_0(-N_1+N_2)d'e'$	$q = 48kI_0N_1d'd'$ $s = 48kI_0N_1e'e'$
$C_{2v}(110)$:B_1	$D_2[110]$:B_2	$s_1 = 8kI_0N_1f'f'$ $s_2 = 2kI_0(2N_1+N_{13}+N_{14})f'f'$ $t_1 = 2kI_0(-N_{13}+N_{14})f'f'$	$s = 8kI_0N_1f'f'$
$C_{2v}(110)$:B_2	$D_2[110]$:B_3	$s_1 = 8kI_0N_1ff$ $s_2 = 2kI_0(2N_1+N_{13}+N_{14})ff$ $t_1 = 2kI_0(N_{13}-N_{14})ff$	$s = 8kI_0N_1ff$

in good agreement with the above discussion of the bleaching properties of the $H_i^0(I^-I^-)$ defect. Moreover, it is found that the orientation v_{13} was hardly bleached by the uv irradiation since the observed intensity $I_{x,yz}$ after the excitation is still more than 50% of its value before the bleaching [compare Fig. 3(c) with 3(e)]. If the population number N_{13} was unaltered by the bleaching, and taking into account the results in Eqs. (5), the intensity $I_{x,yz}$ would be reduced to

$$\tfrac{1}{2}(1+N_1/N_{13}) \approx 60\%$$

as can be derived from the formula in Table V.

Because of the production and pulse-anneal results, and because of the consistency of the Raman results with the expected bleaching properties of the $H_i^0(I^-I^-)$ defect with the proposed model in Fig. 1(c), we attribute this Raman peak to the B_2 mode of this defect which possesses $C_{2v}(110)$ symmetry. This corresponds to a representative mode $D_2[110]$:B_3. In this vibration the H_i^0 atom is moving parallel to the face diagonal joining the two I^- impurity ions. In two other crystals, RbBr:I^- and KBr:I^-, it was possible to perform a similar polarized Raman measurement of the $H_i^0(I^-I^-)$ spectrum with qualitatively the same results (see Table IV), although the experimental data are less precise than in RbCl:I^-. The BT analysis could not be applied to the $H_i^0(Br^-Br^-)$ peak in KCl:Br^- (see Table I) because it strongly overlaps with the A_1 peak of the $H_i^0(Br^-)$ defect: The linewidth occurring in this 5-mol % doped crystal is about 7 cm^{-1}.

V. RAMAN TENSORS OF THE E AND A_1 MODES OF THE $H_i^0(Y^-)$ DEFECT

A. Experimental tensor elements

Neither the instrumental efficiency factor k in the Raman scattering intensities [Sec. III, Eq. (1)] nor the absolute concentration of the defects are known. As a result only the relative values of the Raman-tensor elements of the vibrational modes of the same defect can be determined (see also Ref. 6). The Raman tensors $\underline{T}$ for the E mode of a center with $C_{3v}[111]$ symmetry read (see Table V of Ref. 6)

$$\underline{T}_{E(x')} = \sqrt{3}\begin{bmatrix} d' & 0 & -e' \\ 0 & -d' & e' \\ -e' & e' & 0 \end{bmatrix},$$

$$\underline{T}_{E(y')} = \begin{bmatrix} d' & -2e' & e' \\ -2e' & d' & e' \\ e' & e' & -2d' \end{bmatrix}, \tag{6a}$$

while for the A_1 mode

$$\underline{T}_{A_1} = \begin{bmatrix} a' & b' & b' \\ b' & a' & b' \\ b' & b' & a' \end{bmatrix}, \tag{6b}$$

where the tensors are given with respect to the coordinate axes x, y, and z fixed to the $\langle 100 \rangle$ crystal directions. When the tensors are expressed in the local reference frame (x',y',z') of the defect, they take the usual form as given in Ref. 21. In Table V one finds the explicit expressions of the IP, for the A_1 and E modes of a $C_{3v}[111]$ defect, as a function of the Raman-tensor elements and of the population numbers N_n of the center in its different orientations. It is straightforward to determine from these relations the relative values of the diagonal tensor elements with respect to the off-diagonal ones. One finds for the E mode

$$d'/e' = (v_1/t_1)_E = \pm(q/s)_E^{1/2}, \tag{7a}$$

and for the A_1 mode

$$a'/b'=(v_1/t_1)_{A_1}=\pm(q/s)_{A_1}^{1/2} . \tag{7b}$$

Apart from the sign the ratio of the off-diagonal tensor elements of the A_1 and E modes is given by

$$|b'/e'|=(2s_{A_1}/s_E)^{1/2} . \tag{7c}$$

The ratio s_{A_1}/s_E can be obtained from experimental spectra of the type presented in Figs. 2(c) and 2(d) from which the intensities of the A_1 and E modes can be determined. Note that in Eq. (7c) the IP s_E represents one component of the E mode, making that the intensity of the observed E Raman peak is equal to $2s_E$. There is some spread in this ratio depending on the impurity doping concentrations: Higher doping increases the linewidth (Table I) and enhances the $H_i^0(Y^-Y^-)$ concentration (Sec. III). The B_2 mode of this center is resolved but it is possible that its A_1 and B_1 modes contribute to the A_1 and E lines of $H_i^0(Y^-)$ (Sec. V E). One finds, e.g., for RbCl:I^- that

$$s_{A_1}/s_E=0.9\pm0.1 , \tag{8a}$$

which yields

$$|b'/e'|=1.35\pm0.07 . \tag{8b}$$

The ratios d'/e' and a'/b' can be found in Table IV as the experimental v_1/t_1 or $(q/s)^{1/2}$ parameters. One notes that the six crystals studied can be grouped into sets of two crystals with the same pair (X^-,Y^-) of host and impurity halogen. The values of d'/e' are close to each other for crystals with the same pair (X^-,Y^-), specifically

$$d'/e'\approx\begin{cases}-1.0, & (Cl^-,I^-)\\ -0.7, & (Br^-,I^-)\\ -0.4, & (Cl^-,Br^-) .\end{cases} \tag{9}$$

The ratio a'/b' is much smaller, i.e.,

$$a'/b'\approx0.3 \tag{10}$$

for all our crystals, but the experimental data do not possess a sufficient precision, and as a result trends from one crystal to another cannot be determined.

B. Small perturbation analysis

It is instructive to attempt a zero-order description of the $H_i^0(Y^-)$ tensor elements based on the assumption that, compared to the unperturbed H_i^0 center, the Y^- ion in $H_i^0(Y^-)$ represents only a very small perturbation. A small perturbation would be, e.g., an externally applied uniaxial stress. Such stress yields mode splittings of the order of ~1 cm^{-1},[22] and the Raman-tensor elements are not perceptibly changed.

The Raman tensors of the threefold-degenerate T_2 mode of the unperturbed H_i^0 center are of the form

$$\underline{T}_{T_2(x)}=\begin{bmatrix}0&0&0\\0&0&f\\0&f&0\end{bmatrix},$$

$$\underline{T}_{T_2(y)}=\begin{bmatrix}0&0&f\\0&0&0\\f&0&0\end{bmatrix},$$

$$\underline{T}_{T_2(z)}=\begin{bmatrix}0&f&0\\f&0&0\\0&0&0\end{bmatrix}.$$

These tensors are described with respect to the crystal reference frame fixed to the ⟨100⟩ directions. When the orthogonal vibrations are taken along the local axes x', y', and z' defined for a defect symmetry $C_{3v}[111]$, one finds

$$\underline{T}_{T_2(x')}=\frac{1}{\sqrt{2}}\begin{bmatrix}0&0&-f\\0&0&f\\-f&f&0\end{bmatrix},$$

$$\underline{T}_{T_2(y')}=\frac{1}{\sqrt{6}}\begin{bmatrix}0&-2f&f\\-2f&0&f\\f&f&0\end{bmatrix}. \tag{11}$$

$$\underline{T}_{T_2(z')}=\frac{1}{\sqrt{3}}\begin{bmatrix}0&f&f\\f&0&f\\f&f&0\end{bmatrix}.$$

If the perturbation of the Raman tensors of the H_i^0 defect due to the presence of the Y^- impurity were indeed a very small one, one would expect by comparison of Eqs. (6) and (11), for the E mode,

$$d'=0, \quad e'=f/\sqrt{6} , \tag{12a}$$

and for the A_1 mode,

$$a'=0, \quad b'=f/\sqrt{3} , \tag{12b}$$

which means vanishing diagonal elements and a ratio

$$b'/e'=\sqrt{2} \tag{12c}$$

for the off-diagonal elements.

The experimental d'/e' values presented in (9) are in strong disagreement with (12a). This is sufficient to conclude that the Y^- ion does not represent a very small perturbation. Even so, not all the tensor elements are strongly affected. The observed low a'/b' values [see (10)] suggest that the A_1-mode tensor elements are much less changed than the E-mode ones. Also, the experimental ratio $|b'/e'|$ between the elements of the A_1 and E modes as given in (8b) is not very different from the $\sqrt{2}$ value in (12c). Thus it seems that the off-diagonal elements e' and b' which are already comparable to each other and different from zero for the unperturbed H_i^0 center are not strongly influenced by the Y^- ion even though this ion must be considered to induce a substantial perturbation in the sense discussed above. These conclusions will be substantiated below.

C. Calculation of the Raman-tensor elements

Leaving the zero-order approximation one can push the level of the description further by calculating the Raman-tensor elements within the framework of the valence optical theory.[23] In this theory the electronic polarizability of the molecule is written as a sum of the polarizabilities of the H^0—X^- and H^0—Y^- molecular bonds. We write the electronic polarization $\vec{P}$ as

$$\vec{P}=\sum_{i=1}^{4}\alpha_i\vec{E}+\sum_{i=1}^{4}\beta_i\vec{l}_i(\vec{l}_i\cdot\vec{E}) , \tag{13}$$

in which $\vec{l}_i$ is the unit vector from H^0 to the ith halogen ion and $\vec{E}$ is the electric field. In terms of the polarizabilities $\alpha_{||,i}$ and $\alpha_{\perp,i}$ parallel and perpendicular to a bond direction one has $\alpha_i=\alpha_{\perp,i}$ and $\beta_i=\alpha_{||,i}-\alpha_{\perp,i}$. Assuming that α_i and β_i are only a function of the instantaneous magnitude $R_i=|\vec{R}_i|$ of the H^0-halogen distance (this assumption permits changes in the bond directions), one finds the following expressions for the Raman-tensor components. For the unperturbed H_i^0 centers

$$f=\frac{4\sqrt{3}}{9}(\beta'_X-2\beta^0_X/R_0) , \tag{14}$$

and for the singly perturbed $H_i^0(Y^-)$ center

$$\begin{aligned} a'&=\tfrac{1}{3}(\beta'_Y-\beta'_X)+\alpha'_Y-\alpha'_X ,\\ b'&=\tfrac{1}{9}(3\beta'_Y+\beta'_X-8\beta^0_X/R_0) ,\\ d'&=\frac{\sqrt{3}}{3}(\beta^0_Y-\beta^0_X)/R_0 ,\\ e'&=\frac{4\sqrt{3}}{27}\beta'_X-\frac{\sqrt{2}}{18}(5\beta^0_X+3\beta^0_Y)/R_0 . \end{aligned} \tag{15}$$

In Eqs. (14) and (15) the symbols have the following meanings:

$$\begin{aligned} \alpha_i^0&=\alpha_i(R_0) ,\\ \beta_i^0&=\beta_i(R_0) ,\\ \alpha'_i&=\left[\frac{d\alpha_i}{dR_i}\right]_{R_i=R_0} ,\\ \beta'_i&=\left[\frac{d\beta_i}{dR_i}\right]_{R_i=R_0} , \end{aligned} \tag{16}$$

where R_0 is the hydrogen-halogen equilibrium distance ignoring the difference between H^0-X^- and H^0-Y^- distances. These parameters are not known and they are hard to calculate theoretically. We will attempt to make some guesses about their relative magnitudes so as to arrive at the correct signs of the Raman-tensor elements a',b',d',e'.

Electronic polarizabilities are positive numbers and because it is found experimentally for diatomic molecules[24] that $\alpha_{||}>\alpha_\perp$ it follows that $\beta^0_X,\beta^0_Y>0$. Furthermore, because the polarizabilities of the heavier Y^- halogen ion are larger than the X^- ones[25] it is not unreasonable to assume that $\beta^0_Y>\beta^0_X$. Using these assumptions one concludes from Eqs. (15) that

$$d'\geq 0 . \tag{17}$$

The experimental data on the A_1 mode (Table IV) indicate that the a' parameter is small as given by (10). This means either that the derived polarizabilities α'_i and β'_i are comparable to each other and/or that they are small in the sense that

$$|\alpha'_i|,|\beta'_i|<\beta^0_i/R_0 . \tag{18}$$

Accepting these inequalities one derives from Eqs. (15) that

$$\begin{aligned} b'&\leq 0\\ e'&\leq 0 . \end{aligned} \tag{19}$$

This yields together with (17) that

$$\begin{aligned} e'/d'&\leq 0 ,\\ b'/e'&\geq 0 . \end{aligned} \tag{20}$$

The former agrees with experiment and the latter could not be derived from experiment. The sign of a' is not easily guessed from Eq. (15) but because experimentally $a'/b'>0$ one concludes that $a'<0$.

A final quantitative test which gives confidence in the overall reasonableness of the foregoing analysis is supplied by the following relation which is readily derived and ignores only a small term in $\alpha'_Y-\alpha'_X$:

$$\frac{e'}{d'}+\frac{\sqrt{2}}{2}\frac{a'}{d'}-\frac{\sqrt{2}}{2}\frac{b'}{d'}=-\frac{1}{2} . \tag{21}$$

The most reliable set of data in Table IV is supplied by $H_i^0(I^-)$ in RbCl:I^- and inserting this in the left-hand side of Eq. (21) one finds -0.3 which has the correct sign and is reasonably close to the required -0.5 value. If one assumes that there is overlap with the modes of the $H_i^0(Y^-Y^-)$ center (see Sec. V E) one may improve the agreement.

D. Strength of the perturbation

From the foregoing discussion one can attempt a classification of centers from the point of view of Raman scattering as to whether they are weakly, intermediately, or strongly perturbed compared to an unperturbed model defect. To classify as a weakly perturbed defect the mode shifts and/or splittings should be very small, e.g., less than 1% of the mode position, and the Raman tensors should not be perceptibly changed. As mentioned earlier uniaxial stress applied externally to a sample will induce this type of weak perturbation.

For an intermediately perturbed center the mode splittings and shifts may amount to, e.g., 15%, and the change of the relevant Raman-tensor elements determining the intensities of the split modes is such that their relative intensities are within ~20% of the intensities of the unsplit modes in the unperturbed center. The $H_i^0(Y^-)$ center, and most likely the $H_i^0(Y^-Y^-)$ center too, classify as intermediately perturbed centers.

For the strongly perturbed centers the mode shifts and splittings and change in Raman-tensor elements are very much larger. In fact the structure of the center may be drastically altered and only its atomic or molecular constituents are similar to the original unperturbed model center. The Li^+ perturbed H_i^0 center in KCl is an example of such a strongly perturbed center.[20]

E. A_1 and B_1 modes of $H_i^0(Y^-Y^-)$

The doubly perturbed $H_i^0(Y^-Y^-)$ center possesses $C_{2v}(110)$ symmetry and should possess three Raman-

active modes, namely an A_1, a B_1, and a B_2. In order to avoid confusion the A_1 modes of $H_i^0(Y^-)$ and $H_i^0(Y^-Y^-)$ will be denoted in the remainder of this section by $A_1(Y^-)$ and $A_1(Y^-Y^-)$, respectively. In this paper (Sec. IV C 2) only the B_2 mode is resolved and little has been said so far about the other two modes. One should first consider the possibility that the $H_i^0(Y^-Y^-)$ center is a case of a strongly perturbed H_i^0 in the sense as discussed in Sec. V D. This would imply very large shifts in the frequencies of the $A_1(Y^-Y^-)$ and B_1 modes compared to the unperturbed and singly perturbed H_i^0 centers. This might explain the absence of corresponding Raman signals in our measurements. However, we believe that these modes are present but that they are obscured by the E and $A_1(Y^-)$ modes of $H_i^0(Y^-)$ and/or the T_2 mode of H_i^0. Indeed, $H_i^0(Y^-Y^-)$ was classified in Sec. V D as an intermediately perturbed center just as the $H_i^0(Y^-)$. For the latter the E mode is either very near to or overlaps with the T_2 mode of the unperturbed H_i^0 (see Table I). It is therefore not unreasonable to assume that a similar near-degeneracy occurs between, on the one hand, the E and $A_1(Y^-)$ modes of $H_i^0(Y^-)$ and, on the other hand, the B_1 and $A_1(Y^-Y^-)$ modes of $H_i^0(Y^-Y^-)$. It may also be pointed out that $H_i^0(Y^-Y^-)$ is only visible in the more strongly doped samples which also exhibit a substantially increased linewidth (Table I). These increased $A_1(Y^-)$ and E mode linewidths provide an umbrella for the unseen $A_1(Y^-Y^-)$ and B_1 modes. Unfortunately, this contention cannot be checked experimentally because of the difficulty of producing $H_i^0(Y^-Y^-)$ separately (see Figs. 6 and 7).

Qualitative information about the vibrational frequencies of the $H_i^0(Y^-Y^-)$ center can be derived on quite general grounds, making the following assumption: In the perturbed H_i^0 defects the hydrogen atom is sitting interstitially at, or close to the center of the conventional cube (see Fig. 1), and the NN halogen ions are close to the halogen-ion positions in the unperturbed H_i^0 center. As a result the H^0–X^- and the H^0–Y^- bonds are directed along, or nearly along, the $\langle 111 \rangle$ crystal directions. Furthermore, the potential energy which the H^0 atom experiences can be written as a sum of four pair potentials $f_X(R_{HX})$ and $f_Y(R_{HY})$ originating from the H^0–X^- and H^0–Y^- bonds, respectively, in which R_{HX} and R_{HY} are the corresponding internuclear distances between the H^0 atom and the halogen ions.

If in the $H_i^0(Y^-)$ and $H_i^0(Y^-Y^-)$ centers the static displacements of the hydrogen atom and the halogen ions away from their position in the unperturbed H_i^0 are small, one can evaluate the vibrational frequencies in terms of the first and second derivatives of the pair potentials.

One finds for the unperturbed H_i^0 center

$$w_{T_2}^2 = \tfrac{4}{3} f_X'' + \tfrac{8}{3} f_X'/R_0 \,, \tag{22a}$$

for the singly perturbed $H_i^0(Y^-)$ center

$$w_E^2 = \tfrac{4}{3} f_X'' + (\tfrac{5}{3} f_X' + f_Y')/R_0 \,, \tag{22b}$$

$$w_{A_1(Y^-)}^2 = \tfrac{1}{3} f_X'' + f_Y'' + \tfrac{8}{3} f_X'/R_0 \,, \tag{22c}$$

and for the doubly perturbed center $H_i^0(Y^-Y^-)$:

$$w_{B_1}^2 = \tfrac{4}{3} f_X'' + (\tfrac{2}{3} f_X' + 2f_Y')/R_0 \,, \tag{22d}$$

$$w_{A_1(Y^-Y^-)} = \tfrac{2}{3}(f_X'' + f_Y'') + \tfrac{4}{3}(f_X' + f_Y')/R_0 \,, \tag{22e}$$

$$w_{B_2}^2 = \tfrac{3}{4} f_Y'' + (2f_X' + \tfrac{2}{3} f_Y')/R_0 \,, \tag{22f}$$

in which R is the hydrogen-halogen bond length. For reasonable pair potentials, such as the soft sphere potentials derived for the unperturbed H_i^0 center in Ref. 4, one finds that the main contributions in Eqs. (22) originate from the terms containing the second derivatives, f_X'' and f_Y''. Taking into account the experimental results concerning the $H_i^0(Y^-)$ centers, namely that $w_{A_1(Y^-)} < w_E \approx w_{T_2}$, one finds

$$f_X'' > f_Y'' \,.$$

This allows one to conclude that for the vibrational frequencies of the doubly perturbed center $H_i^0(Y^-Y^-)$, the following relations hold:

$$w_{B_2} < w_{A_1(Y^-Y^-)} < w_{B_1} \approx w_E \approx w_{T_2}$$

and

$$w_{B_2} < w_{A_1(Y^-)} \approx w_{A_1(Y^-Y^-)} \,,$$

which are in qualitative agreement with the available experimental data (see Table I).

The relations given above correspond to the following physical picture: In the $A_1(Y^-)$ mode of the $H_i^0(Y^-)$ center [Fig. 1(b)], the vibrational motion of the H^0 atom is along the H^0–Y^- bond. This mode possesses a lower frequency than the E mode because the corresponding H^0–Y^- pair potential is softer than the H^0–X^- one. In the B_2 mode of $H_i^0(Y^-Y^-)$ [see Fig. 1(c)] the H^0 atom moves against two such H^0–Y^- bonds, and this yields a lower vibrational frequency than the B_1 mode in which the hydrogen atom motion is against two H^0–X^- bonds. Finally, in the $A_1(Y^-Y^-)$ mode of this defect, the H^0 motion is beating partly against the H^0–X^- and the H^0–Y^- bonds, yielding a frequency in between the B_1 and B_2 modes.

VI. CONCLUDING REMARKS

The results presented in this paper concerning the perturbed $H_i^0(Y^-)$ and $H_i^0(Y^-Y^-)$ centers in alkali halides provide a particularly nice example of the possibilities offered by the BT analysis of polarized Raman scattering spectra, the theory of which was presented in the preceding paper.[6] Even though one knew already in this case from electron-spin-resonance measurements the C_{3v} symmetry of the $H_i^0(Y^-)$ center, we have derived with a high level of confidence the same conclusion from the Raman data presented here. This is partly due to the fortunate circumstance that one is able to produce a rather strong anisotropy in the orientation of the centers which can be monitored in optical absorption. By its nature the BT analysis yields not only the symmetry of the defect but also identifies the nature of the vibrational modes and gives valuable information about the Raman-tensor elements.

Even for defects, as is the case here, where a rather

complete BT analysis is possible the information does not come easy: very careful measurements must be performed. For many centers the data may be less complete and less definite conclusions may be drawn. Still the results may be quite valuable when combined with data obtained with other experimental techniques. An example of the latter case is provided by the Li^+ perturbed H^0 center in KCl, the Raman BT results of which will be published in a planned forthcoming paper.[20]

ACKNOWLEDGMENTS

The authors wish to thank A. Bouwen for expert experimental assistance and J. M. Spaeth and L. O. Schwan for supplying some of the crystals. Financial support of the IIKW (Interuniversitair Instituut voor Kernwetenschappen) and of the Geconcerteerde Acties is gratefully acknowledged.

---

*Permanent address: Physics Department, Beijing University, Beijing, China.

[1]A. A. Maradudin, Solid State Phys. 19, 1 (1966).
[2]E. Goovaerts and D. Schoemaker, Phys. Status Solidi B 88, 615 (1978).
[3]E. Goovaerts, L. De Schepper, and D. Schoemaker, J. Phys. (Paris) 41, C6-472 (1980).
[4]E. Goovaerts, L. De Schepper, A. Bouwen, and D. Schoemaker, Phys. Status Solidi A 59, 597 (1980).
[5]E. Goovaerts, J. F. Zhou, and D. Schoemaker, Radiat. Def. 72, 81 (1983).
[6]J. F. Zhou, E. Goovaerts, and D. Schoemaker, preceding paper, Phys. Rev. B 29, 5509 (1984).
[7]J. Rolfe, Phys. Rev. Lett. 1, 56 (1958).
[8]C. J. Delbecq, B. Smaller, and P. H. Yuster, Phys. Rev. 104, 599 (1956).
[9]F. Kerkhoff, W. Martienssen, and W. Sander, Z. Phys. 173, 184 (1963).
[10]F. Fisher, Z. Phys. 204, 351 (1967).
[11]G. Kurz, Phys. Status Solidi 31, 93 (1969).
[12]J. M. Spaeth and M. Sturm, Phys. Status Solidi 42, 739 (1970).
[13]J. M. Spaeth and H. Seidel, Phys. Status Solidi B 46, 323 (1971).
[14]J. M. Spaeth, Z. Phys. 192, 107 (1966).
[15]M. H. Wagner and J. M. Spaeth, Solid State Commun. 14, 1101 (1974).
[16]F. Lohse, G. Reuter, and J. M. Spaeth, Phys. Status Solidi B 89, 109 (1978).
[17]L. O. Schwan, H. J. Paus, R. Bauer, J. M. Spaeth, Semicond. Insul. 5, 92 (1980).
[18]L. O. Schwan, W. Geigle, and H. Paus, Z. Phys. B 35, 43 (1979).
[19]L. O. Schwan, W. Geigle, W. Nagel, R. Bauer, and H. Stall, J. Phys. (Paris) 41, C6-408 (1980).
[20]W. Joosen, J. F. Zhou, E. Goovaerts, and D. Schoemaker (unpublished).
[21]R. Claus, L. Merten, and J. Brandmüller, *Springer Tracts in Modern Physics* (Springer, Berlin, 1975), Vol. 75.
[22]W. Kuch, Diplomarbeit, University of Stuttgart (1977).
[23]L. M. Sverdlov, M. A. Kovner, and E. P. Krainov, *Vibrational Spectra of Polyatomic Molecules* (Wiley, New York, 1974), Chap. II.
[24]*Zahlenwerte und Funktionen,* Vol. I of the *Landolt-Bornstein Series,* edited by A. Eucken and K. H. Hellwege (Springer, Berlin, 1951), Pt. 3, pp. 510ff.
[25]C. Kittel, *Introduction to Solid State Physics,* 5th ed. (Wiley, New York, 1976), p. 411.